Two-dimensional electron mobility limitation mechanisms in $Al_xGa_{1-x}N/GaN$ heterostructures

M. N. Gurusinghe, S. K. Davidsson, and T. G. Andersson

Applied Semiconductor Physics-MBE, Microtechnology and Nanoscience MC2, Chalmers University of Technology, SE-412 96 Göteborg, Sweden

(Received 21 October 2004; revised manuscript received 14 March 2005; published 8 July 2005)

We analyze electron scattering from phonons, ionized impurities, line dislocations, and interface roughness at an $Al_xGa_{1-x}N/GaN$ interface. These mechanisms are responsible for mobility limitations in a two-dimensional electron gas. Scattering from charged dislocation lines, ionized impurities, and surface roughness are added to the lattice scattering processes. The dislocation line scattering is described by a new analytical model for the two-dimensional electron scattering. The total mobility variations with temperature, 10–500 K, and electron concentration, $0.05–2\times10^{13}$ cm^{-2}, were analyzed. Calculations were compared with available and own experimental data in the temperature range 10–300 K. At temperatures below 50 K the ionized impurity scattering and line dislocation scattering were found to limit the mobility. For temperatures at and above room temperature the optical phonon scattering was predominant. For samples having a rough interface between the AlGaN top layer and the GaN channel there was additional roughness scattering at both high and low temperatures. Therefore, to utilize the heterostructures in field effect transistors, operating at high power levels at or above 300 K, several parameters must be carefully controlled. For a two-dimensional electron gas concentration of 1×10^{13} cm^{-2} with mobility above 1500 cm^2/V s at room temperature, the ionized impurities should be less than 1×10^{17} cm^{-3} and the line dislocation density below 1×10^{10} cm^{-2}. Further, the root-mean-square value of the surface roughness need to be less than 1 nm with the lateral surface roughness correlation length larger than 5 nm.

DOI: 10.1103/PhysRevB.72.045316 PACS number(s): 73.40.−c

I. INTRODUCTION

The semiconductors GaN, AlN, and InN, together with the AlGaN and InGaN alloys and their heterostructures, are all important in several photonic and electronic applications. Examples are light emitters covering the UV and the visible range, and high temperature and high power microwave electronics. The basis for these applications is the large and direct band gap of GaN. This provides high breakdown voltage and the ability to sustain large electric fields. The GaN based layers have large piezoelectric constants and high spontaneous polarization both contributing to a built-in electric field.[1] The layers are usually grown by epitaxial methods such as metalorganic vapor phase epitaxy (MOVPE) and molecular beam epitaxy (MBE). The temperatures are quite different as growth takes place at 1050 °C for MOVPE and 750 °C for MBE.

The layers with wurtzite structure are generally grown on sapphire, SiC or Si(111). However, the mismatches in lattice constant and thermal expansion coefficient enhance the development of structural defects such as line dislocations, with densities from 5×10^8 to 5×10^{10} cm^{-2}, and crystallites, 10–100 nm in sizes. Electron scattering from dislocations in bulk GaN has been studied by both modeling and experiments.[2,3] The dislocations propagating through a two-dimensional electron gas (2DEG) have an increasing contribution to the scattering when the dislocation density increases and carrier concentration decreases.[4,5]

Crystallites are less pronounced in epitaxial layers grown at the highest temperatures and for increasing thicknesses. The defects give a nonplanar growth front, which results in a structural morphology of the AlGaN/GaN heterointerface. When this is used for confining a 2DEG the roughness will contribute to the scattering of electrons. Due to the sophisticated modeling needed to describe the mobility, there have been different attempts to simplify the representation. The scattering potential is believed to originate in islands sticking up from an atomically smooth surface. In one model, the 2DEG potential well was simplified to a square quantum well (QW).[6] The roughness, Δ, was described by a random stepwise function. The local energy level fluctuations led to a simple expression of mobility,[6] $\mu(\Delta,L)$, where L is the well width. This model, however, does not work for $\Delta\to0$. To simplify the calculated description of the roughness a Gaussian correlation function with two parameters, Δ for height and λ for lateral distance, is frequently used. In a recent study[5] of the roughness scattering at low temperatures, the roughness correlation heights, Δ, and lateral sizes, λ, were estimated to be 0.3–3.4 nm and 1.5–20 nm, respectively.

Apart from the roughness there is scattering in the 2DEG due to background charges and the Al-concentration in the $Al_xGa_{1-x}N$-barrier. In another study[7] of both MBE and MOVPE samples the island heights were found to be 0.5–2.0 nm for x=9–31%. Mobilities were 10^3–10^4 cm^2/V s for low Al content. As the Al content increased to 31% the mobility decreased below 300 cm^2/V s.[7,8] An increase of the Al in the barrier layer induces a higher sheet charge density due to the higher piezoelectric field, but also reduces the mobility due to the roughness. Too high interface roughness could cause localization of low-lying electron levels. Another important parameter is the distance between the position of the charge distribution and the interface. For increased charge density the maximum, $|\psi|_{max}$, moves toward the interface and thus enhances the roughness scattering.[9] The distance of $|\psi|_{max}$ to the interface was estimate to be above 2 nm for n_{2D}=1

 ©2005 The American Physical Society

$\times 10^{12}$ cm^{-2} and $\sim$0.6 nm for 2×10^{13} cm^{-2}, which is within the typical expected values for surface roughness, Δ.

Mobility calculations are essential when studying the mechanisms limiting the electron transport in a two-dimensional channel at the AlGaN/GaN interface. Clearly, the control of the electron scattering is indispensable for the material and device physics as well as for the design of heterostructure devices. In this work we have studied the effect of different scattering mechanisms on the mobility in the AlGaN/GaN heterostructures. In our analysis the temperature and the 2DEG concentration were used as parameters. A new analytical expression to calculate the dislocation line scattering in two dimensions is presented. To limit the number of parameters the dependence on the Al-concentration in the barrier was omitted. Calculations were used to characterize experimental data. We draw conclusions about the interface properties in order to use the structure for heterostructure field effect transistor (HFET) devices working at and above room temperature.

The paper is organized in the following way. First we describe the experimental techniques used to study mobility and the interface roughness. In Sec. III the mathematical models for the different scattering mechanisms including phonon scattering, dislocation scattering, ionized impurity scattering and interface roughness scattering are given. In Sec. IV the contributions from the scattering models are presented. In Sec. V the scattering contributions are added to describe four different experimental temperature-dependent mobility data.

II. EXPERIMENT

In this section the structural parameters of interest for the 2DEG mobility in the AlGaN/GaN heterostructure are described and experimentally investigated. The following material properties have been studied: 2DEG mobility, 2DEG density, ionized impurity concentration, line dislocation density, and interface roughness.

The AlGaN/GaN heterostructure samples characterized in this work were grown by molecular beam epitaxy on sapphire substrates. The nitrogen atoms were supplied from an Oxford CARS-25 rf-plasma source while Ga and Al came from solid source effusion cells. The growth started with nitridation[10] followed by deposition of a 50 nm thick AlN nucleation layer, setting up the surface for growth of Ga-face GaN. This bulk layer was grown up to a thickness of 1.4 μm. Finally, a heterostructure interface was obtained by growing a 40 nm thick $Al_{0.30}Ga_{0.70}N$ on top of the GaN.

The 2DEG mobility and density were measured by Hall effect using the van der Pauw technique and a typical room temperature 2DEG density was $\sim 2\times 10^{13}$ cm^{-2}. The 2DEG mobility was also measured as a function of temperature. The space charge concentration was investigated[11] by capacitance-voltage profiling (*CV*). This gave a charge density, $(N_D - N_A)$, of $\sim 5\times 10^{17}$ cm^{-3}, where N_D is the donor concentration and N_A is the acceptor concentration, respectively. Typical compensation, (N_A/N_D), values for bulk materials[2] have been found to be in the range 0.3–0.6. The depletion area at the Schottky contact is partially removing electron from the dislocations. Therefore, we assume that the effect of the dislocation line on the *CV* measurement is small.

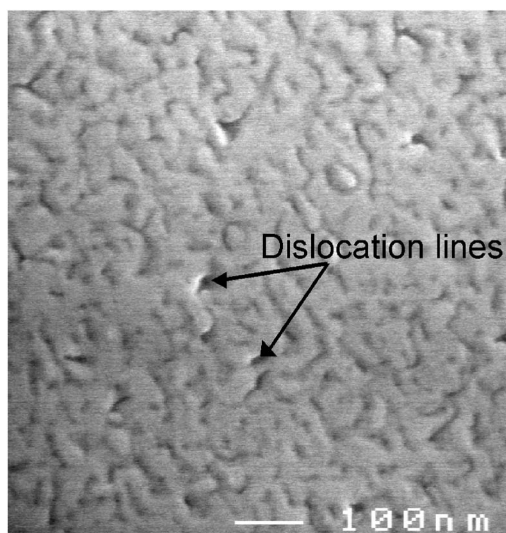

FIG. 1. A SEM image of an AlGaN/GaN sample surface. The dark areas are voids produced by the edge of dislocation lines. These voids are counted to get the dislocation density. In this micrograph the density was $\sim 1\times 10^{10}$ cm^{-2}.

Scanning electron microscopy (SEM) measurements were made to obtain the line dislocation density.[12] A micrograph of a sample surface is shown in Fig. 1. The pits in the figure are considered to be voids originating from the ends of line dislocations. By counting these the sample dislocation density was found to be approximately 1×10^{10} cm^{-2}. Our MBE grown samples had dislocation densities in the range from 5×10^{9} to 5×10^{10} cm^{-2}.

During the growth slightly misaligned GaN crystallites grow in parallel to form the film. The interface roughness is a feature that emanates from the growth process. The roughness of the interface between the AlGaN and GaN contributes to the scattering by a local variation of the width of the quantum well where the 2DEG is confined. Clearly, it is not possible to measure on the interface directly. Instead we estimate the interface roughness by measuring the surface roughness of GaN and AlGaN/GaN samples. Since we have not observed any significant surface smoothing/roughening effect during growth interruption at our growth temperature, it is reasonable to assume that the measured values are representative for the AlGaN/GaN interface roughness. The measurements were made by atomic force microscopy (AFM). The root-mean-square (RMS) value for the height variations is used as a qualitative measure of the surface roughness. The RMS values measured on our MBE grown samples ranged from 0.8 to 5.0 nm.

The surface roughness can be statistically described by using a correlation function defined as $C(\Delta(r)) = \langle\Delta(r)\Delta(r')\rangle = \int \Delta(r+R)\cdot\Delta(r'+R)dR$, where $\Delta(r)$ is the displacement of the interface (height of interface roughness) at position r. For a real sample this correlation function can be numerically calculated from an AFM measurement. However, when the correlation function is to be used in calcula-

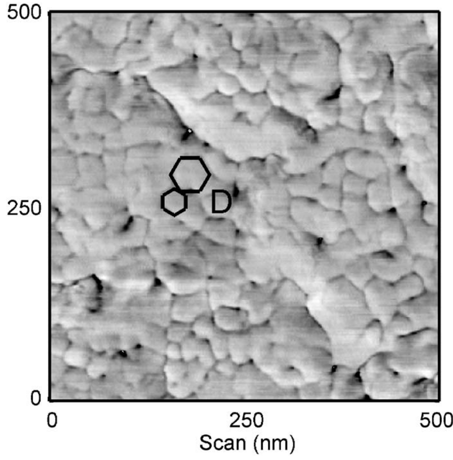

FIG. 2. High resolution AFM tapping-mode measurement. The lateral crystallite size, D, is ranging from 20 to 50 nm. The sample surface roughness (RMS) is 4.5 nm. The figure also shows the voids (black pits) formed by line dislocations (see Fig. 1).

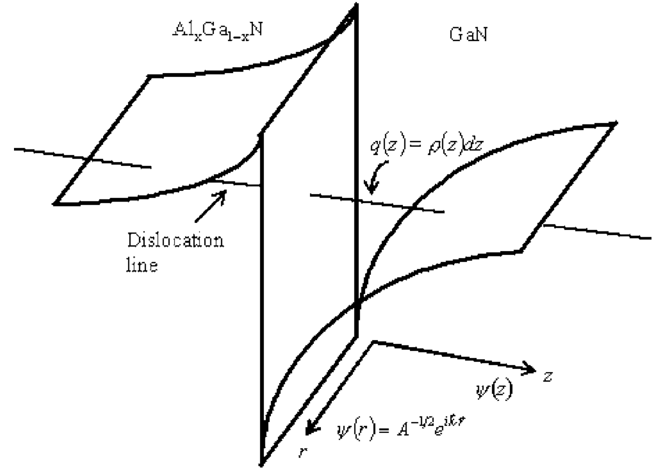

FIG. 3. An illustration of energy band bending at the interface. A dislocation passing through the $Al_xGa_{1-x}N/GaN$ interface is shown as a line.

tions the common and convenient approach is to approximate it with a Gaussian distribution[13] given by

$$\langle \Delta(r)\cdot\Delta(r')\rangle \approx \Delta^2\cdot \exp\left[-\frac{(r-r')^2}{\lambda^2}\right]. \quad (1)$$

Here Δ is, by definition, the RMS value measured by AFM and the parameter λ describes the lateral extension of the height correlation.

Figure 2 shows an AFM image of a surface, which is typical for our samples presented in this work. The morphology is given by crystallites having diameters, D, in the range of 20–50 nm. A complete statistical description of this surface requires two correlation functions, $C_1(\Delta_1,\lambda_1)$ and $C_2(\Delta_2,\lambda_2)$, where C_1 gives the roughness on top of the crystallites and C_2 describes the height variations and distance between neighboring crystallites. The lateral parameters are chosen with respect to the surface features as $\lambda_1 < D$ and $\lambda_2 > D$. The height parameters should add up to the total RMS value as $\Delta^2=\Delta_1^2+\Delta_2^2$. From the AFM data of Fig. 2 we get the parameters $\Delta_1 \approx 1$ nm, $\Delta_2 \approx 4.4$ nm, $\lambda_1 < 20$ nm, and $\lambda_2 > 50$ nm.

III. SCATTERING MECHANISMS

A. Basic consideration

In a pure, defect free material the electron mobility is mainly limited by the electron-phonon interactions. For a real sample the mobility is further reduced by structural defects/impurities that interact with the electrons. Compared to other semiconductors, the nitrides have a special defect in the negatively charged dislocation lines. Since they propagate through heterointerfaces, they may also contribute to the interface roughness. Figure 3 illustrates the energy band bending at the AlGaN/GaN interface and a dislocation propagating through the potential well. Scattering by charge dislocation lines can be categorized, similar to ionized impurities, as a charge impurity scattering.[4]

Several approaches to calculate the two-dimensional electron scattering at semiconductor heterojunction interfaces have been presented.[15–18] However, the calculated values may differ from each other, depending on the theoretical model adopted.[15] Therefore, we briefly describe our calculation procedure and the models used for each scattering mechanism.

As illustrated in Fig. 3 we assume that the two-dimensional electrons are characterized by a plane wave parallel to the AlGaN/GaN interface (in the $\mathbf{r}$-direction) and a quantized wave perpendicular to the interface (in the z-direction). For such a system, the total wave function can be written as $\Psi(r,z)=A^{-1/2}\psi(z)\exp(i\mathbf{k}\cdot\mathbf{r})$, where A is the two-dimensional normalization constant that converts the scattering rate per area. Let us consider a scattering of an incident wave, $\Psi_i(r,z)=A^{-1/2}\psi(z)\exp(i\mathbf{k}\cdot\mathbf{r})$, by a three-dimensional scattering potential $V(r,z)$. After the collision, the scattered wave can be expected to have the form $\Psi_s(r,z)=A^{-1/2}\psi(z)\exp[i(\mathbf{k}+\mathbf{q})\cdot\mathbf{r}]$ with an additional momentum $\hbar q$. The change of wave vector, q, for elastic collisions is given by $q=2\sqrt{2m^*\hbar^{-2}E}\sin(\theta/2)$. Then the matrix element for the transition, $M_{i\to s}=\int\Psi_s^* V(\vec{r},z)\Psi_i dz d\mathbf{r}$, is

$$M_{i\to s}=A^{-1}\int \psi^*(z)[V(r,z)\exp(-i\mathbf{q}\cdot\mathbf{r})d\mathbf{r}]\psi(z)dz, \quad (2)$$

where the middle part of the above equation is the two-dimensional Fourier transform of $V(q,z)$, the relevant potential to describe the two-dimensional scattering, with respect to r for a given z. Therefore we may write the matrix element [given in Eq. (2)] as

$$M_{i\to s}=A^{-1}\int \psi^*(z)[V(q,z)]\psi(z)dz. \quad (3)$$

The energy dependent scattering rate, $\tau^{-1}(E)$, under the assumption that all collisions are elastic, is used for each contribution, and the fundamental equation for a two-dimensional electron gas is[13]

$$\frac{1}{\tau_j(\theta,E)} = \frac{A}{(2\pi)^2}\left(\frac{2\pi}{\hbar}\right) \times \int_{\theta,k'} \left(\frac{M_{j_{i\to s}}}{S(q,T)}\right)^2 (1-\cos\theta)\delta(E_{k'}-E_k)d^2k', \tag{4}$$

where, j denotes the various possible scattering mechanisms. Following Ref. 15, the 2D screening effect is introduced by dividing the scattering matrix element, M_j, by the screening function, $S(q,T)$, where

$$S(q,T) = 1 + \frac{e^2F(q)\Pi(q,T,E)}{2\varepsilon q}. \tag{5}$$

Here the form factor, $F(q)$, is

$$F(q) = \int_0^\infty \int_0^\infty \psi^2(z)\psi^2(z')\exp(-q|z-z'|)dzdz' \tag{6}$$

and $\Pi(q,T,E)$, the polarizability function, is

$$\Pi(q,T,E) = \frac{m^*}{4\pi\hbar^2 k_B T}\int_0^\infty \frac{1-\Theta(q-2k_F)[1-(2k_F/q)^2]^{1/2}}{\cosh^2[(E_F-E)/2k_BT]}dE. \tag{7}$$

In this equation $\Theta(x)$ is representing the usual step function. Next, the total scattering is calculated from the time constant values (as a function of energy, E)

$$\tau(E) = \left(\sum_j \tau_j^{-1}(E)\right)^{-1}. \tag{8}$$

At the end, the numerically calculated energy-dependent scattering time is averaged according to the Fermi statistics, which is given by

$$\langle\tau\rangle = \int \tau(E)E\frac{\partial f_\circ(E)}{\partial E}dE \Bigg/ \int E\frac{\partial f_\circ(E)}{\partial E}dE. \tag{9}$$

This is valid for both nondegenerate and degenerate electron densities. Here E is energy and $f_\circ$ is the Fermi function. The measurable quantity, the mobility, which connects the material and structural quantities through the scattering rates, is calculated from the well-known relation

$$\mu(T,n_{2D},P_i) = \frac{e}{m^*}\langle\tau(T,n_{2D},P_i)\rangle. \tag{10}$$

Equation (10) allows us to study the mobility as a function of temperature T, electron concentration n_{2D} and other various structural and material parameters denoted by P_i. We have focused on two-dimensional (2D) electron scattering at heterointerfaces due to phonons, charged impurities, line dislocations, and surface roughness; all of which are included in our calculations. Further, the Fang-Howard variational wave function,[14] $\psi(z)=(b^3z^2/2)^{1/2}\exp(-bz/2)$, was used to calculate the scattering matrix elements. Here the variational parameter, b, is given by $b=(12m^*e^2n/\varepsilon\hbar^2)^{1/3}$, where $n=(N_{depl}+11/32\times n_{2D})$ and n_{2D} and N_{depl} are the two-dimensional electron density in the channel and the depleted electron concentration in the barrier region, respectively.

After these basic considerations of the physical system we treat the scattering mechanisms one by one as follows.

B. Phonon scattering

The electron-phonon (e-ph) interactions usually depend on the physical parameters of the material rather than on its structure. However, the e-ph scattering time constant depends on the electron density in the channel via the wave function and the electron distribution statistics. Phonons are the major source of scattering at high temperature and may even dominate at low temperatures in very pure materials. Two types of e-ph scattering mechanisms are expected. First, there is the acoustic phonon scattering, which has the two modes, *deformation potential scattering* and *piezoelectric potential scattering*. Second, we have the *optical phonon scattering*. The scattering time constants for these three are given here and the calculated results are given in Sec. IV.

The scattering time constant due to the *deformation potential scattering* is given by[15,19]

$$\frac{1}{\tau_{dp}(\theta,E)} = \frac{3bE_{dp}^2 m^* k_B T}{32\pi\hbar^3 C_L}\int \frac{(1-\cos\theta)}{S^2(q,T)}d\theta. \tag{11}$$

Here E_{dp} is the deformation potential and C_L is the longitudinal elastic constant.

The analytical formula for the *piezoelectric scattering* is[15,20]

$$\frac{1}{\tau_{pe}(\theta,E)} = \frac{(eh_{14})^2 m^* k_B T}{4\pi\hbar^3} \times \int \frac{(1-\cos\theta)}{qS^2(\theta,E)}\left[\frac{9}{32C_L}f_L(y) + \frac{13}{32C_T}f_T(y)\right]d\theta. \tag{12}$$

The parameter h_{14} is a piezoelectric tensor element and C_T is the transverse elastic constant. The expressions for the factors $f(y)$ are, for the longitudinal phonons, $f_L(y)=(1+6y+12y^2+2y^3)/(1+y)^6$ and for the transverse phonon mode, $f_T(y)=(13+78y+72y^2+82y^3+36y^4+6y^5)/13(1+y)^6$, respectively, with $y=q/b$. Here, q is the change of the electron wave vector at the scattering event and b is the variational parameter described with the wave function in Sec. III A.

Since the electron scattering by *optical phonons* is an inelastic process, only approximate analytical expressions has been given in the literature. From those, we adopt the results by Hirakawa *et al.*[15] In this approach, the scattering time was derived by neglecting the in-scattering term (thus the inelastic scattering is maintained) and is given by

$$\frac{1}{\tau_{po}(\theta,E)} = \frac{e^2 m^*\hbar\omega_{LO}(\varepsilon_\infty^{-1}-\varepsilon^{-1})}{8\pi^2\hbar^3[1-f_\circ(E)]} \times \int (1-\cos\theta)\{[1-f_\circ(E+\hbar\omega_{LO})]N_q I(q_{\|+}) + [1-f_\circ(E-\hbar\omega_{LO})] \times \Theta(E-\hbar\omega_{LO})(N_q+1)I(q_{\|-})\}d\theta. \tag{13}$$

Here $\hbar\omega_{LO}$ denotes the longitudinal optical (LO) phonon en-

ergy, ε_∞ is the optical or high frequency dielectric constant, $q_{\parallel +}$ and. $q_{\parallel -}$ are the scattering wave vectors in the phonon absorption and emission, respectively. The phonon occupation number, N_q, is given by $N_q=[\exp(\hbar\omega_{\rm LO}/k_BT)-1]^{-1}$. The quantity $I(q_{\parallel\pm})$ is defined as $I(q_{\parallel\pm})=\int(q_{\parallel\pm}^2+q_z^2)^{-1}|I(q_z)|^2dq_z$, where $I(q_z)^2=b^6/(b^2+q_z^2)^3$ for the Fang-Howard wave function.

The mobility values as a function of temperature and 2DEG concentration have been calculated from these expressions and they are presented in Sec. IV.

C. Charged impurity scattering: Dislocations and ionized donors

Let us consider an elemental charge with density $\rho(z_i)$ at the position z_i along the dislocation line (cf. Fig. 3). The Coulomb potential is given by $dV(r,z_i)=e\rho(z_i)dz_i/4\pi\varepsilon\sqrt{z_i^2+r^2}$. Our next step is to Fourier transform this potential and substitute it into Eq. (3). This can be done by considering this elemental charge as a point charge and using two-dimensional Fourier-Bessel functions.[13] The Fourier transformed potential can then be written as

$$dV(q,z_i)=\frac{2\pi e}{4\pi\varepsilon}\frac{\rho(z_i)\exp(-qz_i)dz_i}{q}. \tag{14}$$

After substituting Eq. (14) into Eq. (3), the matrix element becomes

$$M_{i\to s}=\frac{eA^{-1}}{2\varepsilon}\int_z\psi^*(z)\left[\int_{z_i}\rho(z_i)\left(\frac{\exp(-q|z_i-z|)}{q}\right)dz_i\right]\psi(z)dz. \tag{15}$$

The analytical expression for the *dislocation scattering* time constant, under the assumption that all collisions are elastic, can be obtained by substituting Eq. (15) into Eq. (4) and multiplying by the dislocation density. In order to calculate the dislocation charge density $\rho(z)$, we substitute $\rho=ef/c$ in Eq. (15), where a constant filling of electrons into the dislocation line (with a degenerate state[2,3] in the band gap), is assumed. Here f is the filling factor,[2] c is the lattice constant, and $N_{\rm dis}$ is the areal dislocation density, respectively. The final analytical expression for scattering time constant is then given by

$$\frac{1}{\tau_{\rm dis}(\theta,E)}=\left(\frac{m^*e^4N_{\rm dis}f^2}{8\pi\varepsilon^2c^2\hbar^3}\right)\times\int_\theta\left\{\int_z\psi^*(z)\left[\int_{z_i}e^{-q|z_i-z|}dz_i\right]\psi(z)dz\right\}^2\times\frac{(1-\cos\theta)}{[qS(q,T)]^2}d\theta. \tag{16}$$

The effect on the transport properties in the 2D channel from ionized impurities has been discussed before.[15] The local potentials of ionized centers rearrange the electrons to screen the impurity charges. To model the *ionized impurity scattering* we use a similar approach as the one used above for dislocation scattering. We rearrange our matrix element given in Eq. (15) by substituting $\rho(z_i)dz_i=eZ$, where Z is the atomic number of the impurity atom. By considering these impurities at a random position, say z_i, the rate of ionized impurity scattering is

$$\frac{1}{\tau_{ii}(\theta,E)}=\left(\frac{m^*e^4Z^2}{8\pi\hbar^3\varepsilon^2}\right)\int_{z_i,\theta}\left[\frac{F(q,z_i)}{qS(q,T)}\right]^2dz_iN_{ii}(z_i)(1-\cos\theta)d\theta, \tag{17}$$

where the form factor is defined by

$$F(q,z_i)=\int|\psi(z)|^2\exp(-q|z_i-z|)dz.$$

This is precisely the result obtained by Hirakawa *et al.*[15] In particular, the dislocation and ionized impurity scattering terms are similar to each other. The scattering potentials are independent of temperature, but there is a dependence in the screening function [see Eq. (5)]. This together with averaging over energy [via Eq. (9)] is expected to provide only a weak temperature dependence for the mobility.

D. Interface roughness scattering

Spatial variations of the interface roughness, $\Delta(r)$, change the wave function and thus the energy levels. These potential fluctuations generate the local potential for the electron scattering. We use the formalism by Ando *et al.*[13] and apply it on the GaN system. The interface roughness gives the scattering potential, $V=\Delta(q)\Gamma(q)$, where $\Gamma(q)=\gamma(q)+\gamma_{\rm image}(q)$. Since the permittivity of the barrier material (AlGaN) and the well material (GaN) is nearly equal, $\gamma_{\rm image}$ is negligible and $\Gamma(q)=\gamma(q)=(e^2/\varepsilon)(n_{2D}/2+N_{\rm depl})$. This is valid for both low and high q values. Clearly the electron scattering from interface roughness not only depends on the height dimension of the roughness, but also on the lateral dimension, $\lambda(r)$. For a real material these features can be quite different from place to place. Therefore, the usual technique is to assume a Gaussian form of the correlation of the surface roughness by statistically defined Δ and λ. Now Δ is the average displacement of the interface and λ is the auto correlation length of Δ, see Sec. II. Finally, the matrix element for scattering has been analytically expressed as

$$\langle|M_{i\to s}|^2\rangle=\frac{e^2\Delta^2\lambda^2}{\varepsilon^2}\exp\left(-\frac{q^2\lambda^2}{4}\right)\left(\frac{1}{2}n_{\rm 2D}+N_{\rm depl}\right)^2, \tag{18}$$

and then the scattering time constant for the interface roughness is given by

$$\frac{1}{\tau_{\rm ir}(\theta,E)}=\frac{m^*(\Delta\lambda)^2}{2\hbar^3}\int_\theta\exp\left(-\frac{q^2\lambda^2}{4}\right)\left[\frac{\Gamma(q)}{S(q,T)}\right]^2(1-\cos\theta)d\theta. \tag{19}$$

The scattering rate is mostly determined by the prefactor $(\Delta\lambda)^2$ and λ in the exponential part. The dependence on the 2DEG concentration is determined by $(n_{\rm 2D}+2N_{\rm depl})^2$ resulting in a decrease of the mobility according to $\mu_{\rm ir}\sim n_{\rm 2D}^{-2}$.

TABLE I. Material parameters used for the calculations. Here $m_\circ$ and $\varepsilon_\circ$ are the rest electron mass and permittivity of free space, respectively.

Parameter	Symbol (units)	Value	Reference
Effective electron mass		$0.22m_\circ$	21
Dielectric constant (low frequency)	ε (F/m)	$10.4\varepsilon_\circ$	22
Dielectric constant (high frequency)	ε_∞ (F/m)	$5.47\varepsilon_\circ$	22
Deformation potential	E_{dp} (eV)	8.5	17
Piezoelectric constant	h_{pz} (C/m^2)	0.5 (0.375–0.6)	22
Longitudinal elastic constant	C_L (N/m^2)	2.65×10^{11}	21
Transverse elastic constant	C_T (N/m^2)	4.42×10^{10}	21
LO-phonon energy	$\hbar\omega_{\mathrm{LO}}$ (meV)	91.2	21
Lattice parameter	c (Å)	5.185	23

IV. CALCULATED RESULTS

In this section we make a detailed analysis of the different scattering mechanisms involved in the 2DEG transport. The scattering contributors are studied with respect to temperature and sheet electron charge density. The multitude of mechanisms can make the analysis of experimental results rather difficult. Therefore the mobility contributions are divided into three groups. First mobility from the electron-phonon scattering is calculated. This is considered to originate from background scattering: as-given for the material. Secondly, contributions from impurities, both dislocation lines and ionized impurities, are treated. The third subject of discussion is the mobility contribution from interface roughness. The basic material parameters put into the calculations are listed in Table I.

Because of the many coupled parameters in real HFET structures, it is not straightforward to independently determine a single quantity. Self-consistent calculations using the Poisson and Schrödinger equations[11] at 300 K, have shown that only the lowest energy state was populated when $n_{2D} < 2\times10^{13}$ cm^{-2}. The confined level is at least $\sim 4k_BT$ below the GaN band edge at room temperature providing a 2DEG.

A. Phonon scattering

First we study the scattering from the lattice. This phonon-scattering is composed of the three contributions described in Sec. III B. In Fig. 4 the mobility contributions from the phonon scattering are given as a function of temperature for a typical 2DEG concentration. At high temperatures, $T > 150$ K, the optical phonon scattering is dominating, whereas for the lower temperature range, $0 < T < 150$ K, the deformation potential scattering dominates.

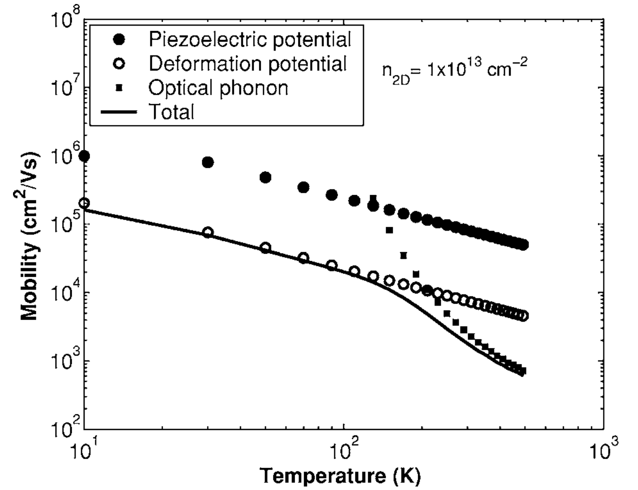

FIG. 4. Mobility as a function of temperature (the 2DEG density is 1×10^{13} cm^{-2}). The solid line represents the resulting mobility from all three scattering contributions. The piezoelectric scattering is small compared to the other two scattering processes.

The piezoelectric scattering has almost no effect on the phonon limited mobility.

Figure 5 shows that, besides being temperature dependent, the phonon scattering contributions vary with the 2DEG density. Our calculations showed that the mobility decreased from 5450 to 1500 cm^2/V s within the carrier concentration range from 5×10^{11} to 2×10^{13} cm^{-2}. This is important, since the density is used as a parameter when fitting calculations to experimental data. In the AlGaN/GaN heterostructure the 2DEG concentration depends on several parameters such as the aluminum concentration in the AlGaN layer,[8] background doping,[11] polarization fields,[23,24] and intentional doping. In the calculations presented here, we do not specify the source of electrons in the 2DEG channel. Also we have excluded the scattering due to the alloy in the

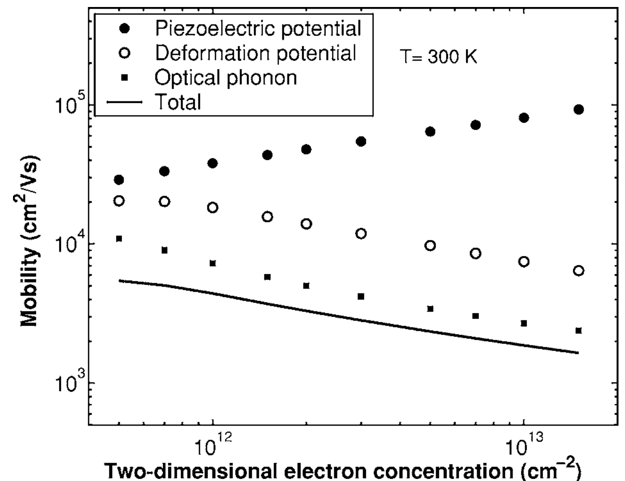

FIG. 5. The variation of the 2DEG mobility at room temperature as a function of the electron concentration for the three different phonon scattering mechanisms. The resulting mobility is shown by the solid line. As shown, the piezoelectric contribution is small, especially at concentrations above $\sim10^{12}$ cm^{-2}.

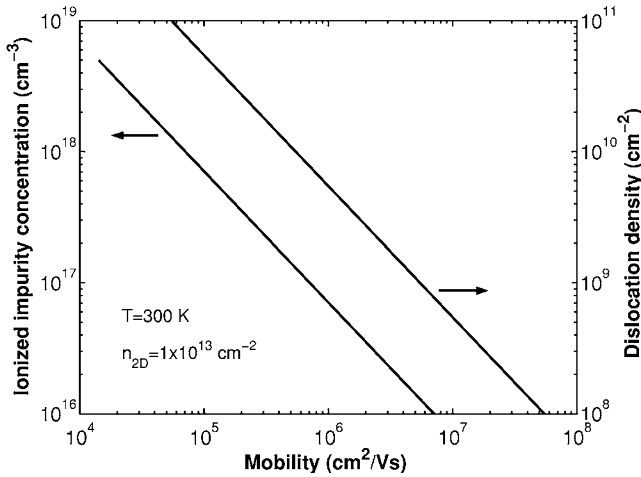

FIG. 6. Mobility dependence on the ionized impurity concentration and dislocation density for a 2DEG at room temperature with 1×10^{13} cm^{-2} electrons.

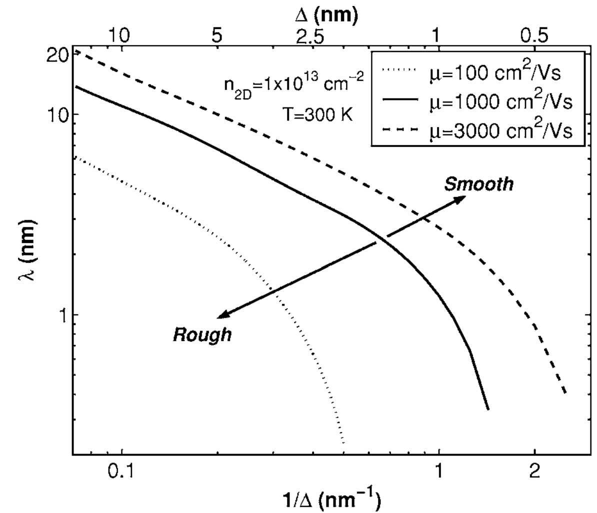

FIG. 7. Calculated mobility contours as a function of the roughness parameters λ and $1/\Delta$. Three constant mobility values, 100, 1000, and 3000 cm^2/V s, are shown for a typical electron concentration at room temperature. The interface morphology is characterized as rough or smooth with reference to $\mu\sim1000$ cm^2/V s.

barrier layer since it is considered to be small in our approach.

Since the phonon scattering processes are as-given by the material, their aggregated contribution to the mobility can be considered as limiting for other scattering mechanisms. That is, scattering from other mechanisms is not important as long as they are small compared to the phonon scattering. In the following paragraphs, critical quality parameters for the impurity scattering and interface roughness scattering mechanisms will be defined to express when they become more important than the phonon scattering.

B. Ionized impurities and dislocations

Unintentional impurities and dislocations are usually an effect of the substrate and growth parameters. The impurities and dislocations are treated much in the same way since their scattering contributions to the overall mobility are similar. In addition it is complicated to discern between their contributions to the free charge concentration.

Atoms and vacancies that have been unintentionally incorporated in the semiconductor are categorized as impurities. These are either neutral or ionized. Whereas the neutral atom scattering is quite small (neglected in this study), the scattering from the ionized impurities is significant, especially at low temperatures. The dislocations are structural defects in the lattice and for the 2DEG mobility the edge dislocation is considered to be the most important. This can act as an electron acceptor[2] with an effective charge density. Despite the difference between edge and screw dislocations we modeled them as line dislocations. In this work we have considered the Coulomb potential as the scattering potential for the line dislocations similar to the ionized impurity potential (see Sec. III C).

Figure 6 shows the mobility calculated from ionized impurity and line dislocation scattering, respectively, for $n_{2D}=1\times10^{13}$ cm^{-2} at room temperature. The filling factor[2] is assumed to be one. The mobility is inversely proportional to both concentrations and there is a strong dependence. The mobility for $N_{dis}<1\times10^{10}$ cm^{-2} is above $\sim6\times10^5$ cm^2/V s. The ionized impurity concentration needed to press its mobility below 6×10^5 cm^2/V s is more than 1.5×10^{17} cm^{-3}.

C. Interface roughness

In this section we discuss the effect of AlGaN/GaN interface roughness on the transport of electrons in the 2DEG. The characteristic of the wave function decides the amount of scattering, which means that the electron scattering is most prominent for the electrons closest to the interface. The interface roughness is statistically modeled by a lateral dimension, λ, and a vertical dimension, Δ. For further information on the model for the scattering potential see Sec. III D. The interface roughness mobility varies with both parameters, λ and Δ. In general terms the mobility increases if Δ decreases and λ increases. As shown in Fig. 7 there is a relation between them, which is illustrated by the mobility contours. With reference to the mobility, 1000 cm^2/V s at room temperature, we categorize the interface morphology as either rough or smooth. A smooth surface provides a mobility above 1000 cm^2/V s. A plot of mobility contours as a function of λ and $1/\Delta$ is shown in Fig. 7. The border between rough ($\mu<1000$ cm^2/V s) and smooth ($\mu>1000$ cm^2/V s) conditions is indicated by the solid line.

For typical values of the surface parameters, $\lambda=4$–5 nm and $\Delta=1$ nm, the mobility contribution from the interface roughness scattering, μ_{ir}, is about 4000 cm^2/V s. This value is also higher than the contribution from the optical phonon scattering, $\mu_{op}\approx2000$ cm^2/V s. On the other hand, at low temperatures the phonon scattering mobility is 100 000 cm^2/V s (Fig. 4), whereas μ_{ir} remains the same. Hence, the roughness has the largest effect on the total mobility at low temperatures.

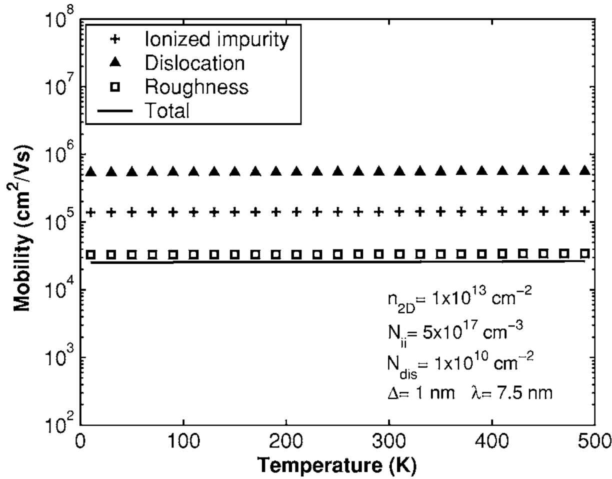

FIG. 8. Temperature dependence of the mobility due to ionized impurity scattering, line dislocation scattering, and interface roughness scattering.

D. Combined mobility

As shown in Fig. 8, there is no significant temperature dependence for the mobility contributions from line dislocations, ionized impurities, and interface roughness. However, it is important to point out that this trivial result is obtained under the assumption that the 2DEG density is independent of temperature. In Fig. 9 the mobility at different 2DEG densities have been calculated for selected parameters. The data shows that the mobility dependencies of the 2DEG concentration due to line dislocation and the ionized impurity contributions increase linearly. The dislocation-limited mobility was calculated assuming completely charged dislocation lines ($f=1$). The interface roughness mobility was calculated for $\Delta=1$ nm and $\lambda=7.5$ nm. As predicted in Sec. III D the roughness mobility decreased with the two-dimensional electron density. The resulting mobility has a maximum due to the two main limiting factors, roughness scattering (at high 2DEG concentrations) and ionized impurity scattering (at low).

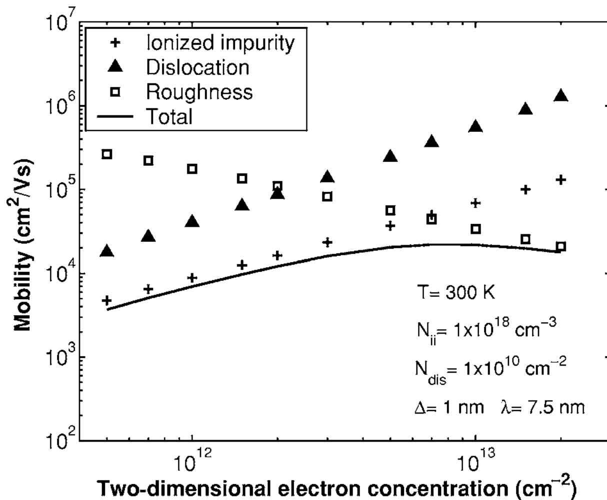

FIG. 9. The mobility dependence on 2DEG density due to ionized impurity scattering, line dislocation scattering, and roughness scattering.

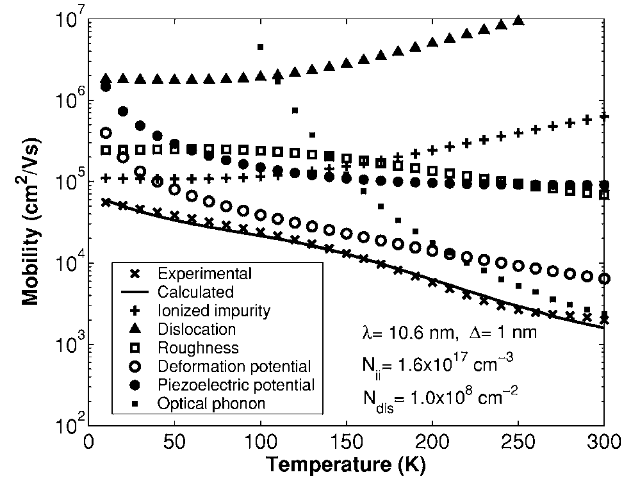

FIG. 10. Measured [from Frayssinet *et al.* (Ref. 25)] (×) and calculated (solid line) mobility data shown as a function of temperature. The contributions from individual scattering mechanisms are also shown. The parameter values used to get the best curve fit are given in the figure.

V. DESCRIPTION OF MEASURED RESULTS AND DISCUSSION

In this section we use our calculations to describe measured mobility data. The results in the previous sections are applied when analyzing experimental data and identifying the dominant scattering mechanisms. An AlGaN/GaN heterostructure grown by MBE were studied together with available Hall effect results.[25–27] The main differences between the samples are the purity of materials and the substrate used.

Figure 10 shows the calculated and measured mobilities for a sample[25] grown on a single crystal GaN substrate by MBE. In addition, the mobility contribution from each considered scattering mechanisms is given. Hall effect measurement gave mobilities of 60 000 cm^2/V s at 1.5 K, 30 000 cm^2/V s at 77 K, and ~2000 cm^2/V s at room temperature. The carrier concentration at room temperature was $\sim 1.5\times 10^{13}$ cm^{-2}. This gradually decreased to $\sim 2\times 10^{12}$ cm^{-2} down to 100 K and remained constant for lower temperatures. In this sample it is evident that the high temperature mobility is given by the optical phonon scattering. The deformation potential contributes at medium temperatures, ~75–150 K, giving a slight bump to the mobility curve. At the lowest temperature the calculated results showed that interface roughness scattering and ionized impurity scattering dominate the mobility. The calculations agreed with the measured values when setting the ionized impurities to 1.6×10^{17} cm^{-3} and tuning the surface roughness parameters to $\lambda=10.6$ nm and $\Delta=1.0$ nm. The contributions from the other scattering events were small for this sample.

In Fig. 11 we present the experimental and calculated mobility data for the high quality sample together with three

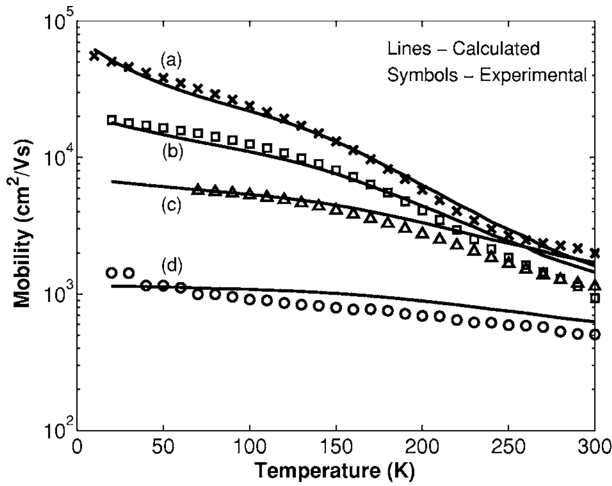

FIG. 11. Mobility as a function of temperature for four selected samples with different mobility. The solid lines are calculated data and the symbols are experimental results. The low temperature mobility span from 1200 to 60 000 cm^2/V s. References for the experimental data are given in Table II.

additional samples.[25–28] All samples were grown by MBE. The material parameter values used in the calculations are given in Table I and the structural parameters are found in Table II. The mobility relation (a) in Fig. 11 is the one given in Fig. 10. In the data set[26] (b) the low temperature mobility was about 20 000 cm^2/V s and the room temperature value was $\sim$1150 cm^2/V s. The 2DEG density varied with temperature. It was $\sim 1.4\times 10^{13}$ cm^{-2} at room temperature and decreased to $\sim 5\times 10^{12}$ cm^{-2} near 100 K and remained constant down to 12 K. The two samples[27,28] (c) and (d) had lower mobilities than (a) and (b) but exhibited constant 2DEG concentration over the studied temperature range. In sample (c) the room temperature mobility was 1211 cm^2/V s and increased to 5660 cm^2/V s at 77 K. The 2DEG concentration was constant at $\sim 5\times 10^{12}$ cm^{-2}. For sample (d) the 2DEG concentration was higher, $\sim 2\times 10^{13}$ cm^{-2}, and the mobility increased from $\sim$500 cm^2/V s at 300 K to $\sim$1400 cm^2/V s at 10 K. The growth details for this sample were presented in Sec. II.

The general mobility dependence on temperature is similar for the four samples in Fig. 11. However, the mobility difference at low-temperature is much larger than at room temperature. This high temperature behavior is because of the dominating contribution from the optical phonon scattering. At low temperature there are structural differences between the samples, which limit the scattering. As shown, the mobility difference between (b) and (c) at high temperature is almost zero while it is significant at low temperature. Our calculations show that the decreased low temperature mobility in (b) and (c) [as compared to (a)] can be explained by an increased interface roughness, which enhances the scattering.

The temperature dependence of the fourth sample (d) differs from the other results. Our calculations showed that the surface roughness scattering explains this deviation. We used the experimental parameter values discussed in Sec. II. However, the surface roughness parameters need to be clarified. The sample in Fig. 2 is representative for sample (d), since they were grown at the same conditions. The discussion in Sec. II demonstrated that the interface roughness in sample (d) was described by two correlation functions, C_1 and C_2. However, the result in Fig. 7 shows that the scattering contribution from the larger surface features, C_2, is comparatively small. Therefore, only C_1, $\lambda < 20$ nm and $\Delta \approx 1$ nm, needs to be considered in the calculations for this sample (d). Due to the limited lateral resolution of the AFM, it was not possible to find an exact value of the correlation length below 10 nm. Instead we used the correlation length as a fitting parameter. The best fit was obtained for $\lambda = 2.23$ nm, which significantly increased the roughness scattering compared to the other samples. The dislocation density, $N_{\mathrm{dis}} = 1\times 10^{10}$ cm^{-2}, and the ionized impurity concentration, $N_{ii} = N_D + N_A \approx 9\times 10^{17}$ cm^{-3}, are high in sample (d). Also the 2DEG density is significantly higher, $n_{\mathrm{2D}} \approx 2\times 10^{13}$ cm^{-2}, than in the other samples. Further, even though these scattering mechanisms are quite large, they are small compared to the surface roughness scattering. In conclusion, the difference between (d) and the other data is explained by the interface morphology parameters.

In Fig. 11 we also notice that there is a deviation between calculations and measurements at room temperature. First we consider samples (a) and (b). Both exhibited temperature de-

TABLE II. Parameters for the calculations of different data shown in Fig. 11. The fitting parameters for sample (d) were supported by experimental data measured on it and samples grown at the same conditions.

	(a)	(b)	(c)	(d)
μ (T_{low})(cm^2/V s)	60 000 (T=1.5 K)	20 000 (T=12 K)	5 660 (T=77 K)	1 300 (T=10 K)
μ (T_{300})(cm^2/V s)	2000	1150	1211	500
n_{2D} (cm^{-2})	0.2–1.5$\times 10^{13}$	0.5–1.4$\times 10^{13}$	5×10^{12}	$\sim 2\times 10^{13}$
Substrate	GaN single crystal	GaN templates by MOVPE	Al_2O_3	Al_2O_3
Grown by	MBE	MBE	MBE	MBE
N_{ii} (cm^{-3})	1–2$\times 10^{17}$	$\sim 1.6\times 10^{16}$	Not specified	$\sim 9\times 10^{17}$
N_{dis} (cm^{-2})	low	Not specified	Not specified	1×10^{10}
Δ (nm)	1	1	1	1
λ (nm)	10.6	5.3	4	2.23
Ref.	25	26	27	28

pendent 2DEG concentrations. The reason was claimed to be parallel conduction which would reduce the mobility.[25,26] However, the calculated mobility was lower than the measured value in sample (a) but higher than the corresponding value in (b). Therefore, sample (a) might not have any parallel conduction. Further, the very low dislocation density in (a) could be a decisive difference between the samples. The calculated mobilities for samples (c) and (d) were higher than the measured values. At 300 K the mobility value is fixed by the LO-phonon energy. We have no evidence for a parallel conduction at room temperature, but we cannot fully exclude a contribution from it. Other effects, which are beyond the scope of this work, such as remote charge impurities in the barrier, piezoelectric and polarization effects, and surface effects are not accounted for in the model.

VI. CONCLUSIONS

The 2DEG electron scattering mechanisms in AlGaN/GaN heterostructures were successfully analyzed and the dominant scattering mechanisms in the low and high temperature regimes were presented. A new analytical model to calculate the time constant for dislocation line scattering as a function of temperature was developed. The interface roughness scattering was carefully analyzed due to its large influence on the mobility in rough samples. The interface can be characterized by its morphology on the scale rough to smooth using statistically defined roughness parameters. The values of them can be derived from AFM measurements.

The highest possible mobility at and above room temperature is determined by optical phonon scattering, which depends on the carrier concentration and material parameters. At low temperatures the mobility is limited by the structural defects such as interface roughness, impurities and dislocations. Hall effect measurement data for four different heterostructures were studied and the measured mobility was reproduced by our calculations. In general terms our study showed that in high mobility samples ($\mu > 60\,000\ \mathrm{cm^2/V\,s}$ at 20 K) the ionized impurity scattering and the interface roughness scattering are limiting the low temperature mobility. In samples with lower mobility ($\mu \sim 20\,000$–$60\,000\ \mathrm{cm^2/V\,s}$) the effect of interface roughness scattering is dominating. At room temperature the optical phonon scattering was the most important limitation when $\mu > 1000\ \mathrm{cm^2/V\,s}$, whereas the interface roughness scattering may reduce the mobility to a value below $1000\ \mathrm{cm^2/V\,s}$.

To be able to use the AlGaN/GaN sample in an application such as a heterostructure field effect transistor, operating at high power levels at or above 300 K, several parameters must be carefully controlled. From our calculated results we conclude that for a two-dimensional electron gas concentration of $1\times 10^{13}\ \mathrm{cm^{-2}}$ with mobility above $1500\ \mathrm{cm^2/V\,s}$ at room temperature, the ionized impurities should be less than $1\times 10^{17}\ \mathrm{cm^{-3}}$ and the line dislocation density is below $1\times 10^{10}\ \mathrm{cm^{-2}}$. Further, the root-mean-square value of the surface roughness need to be less than 1 nm with the lateral surface roughness correlation length larger than 5 nm. These parameter values can serve as a minimum quality measure for application requirements.

[1] F. Bernardini and V. Fiorentini, Phys. Rev. B **64**, 085207 (2001).

[2] M. N. Gurusinghe and T. G. Andersson, Phys. Rev. B **67**, 235208 (2003).

[3] N. G. Weimann, L. F. Eastman, D. Doppalapudi, H. M. Ng, and T. D. Moustakas, J. Appl. Phys. **83**(7), 3656 (1998).

[4] D. Jena, A. C. Gossard, and U. K. Mishra, Appl. Phys. Lett. **76**(13), 1707 (2000).

[5] D. Zanato, S. Gokden, N. Balkan, B. K. Ridley, and W. J. Schaff, Semicond. Sci. Technol. **19**, 427 (2004)

[6] C. Y. Mou and, T. Hong, Phys. Rev. B **61**(19), 12612 (2000).

[7] Y. Zhang, I. P. Smorchkova, C. R. Elsass, S. Keller, J. Ibbetson. S. Denbaars, U. Meshra, and, J. Singh, J. Appl. Phys. **87**(11), 7981 (2000).

[8] Y. Zhang and J. Singh, J. Appl. Phys. **85**(1), 587 (2000).

[9] J. Antoszewski, M. Gracey, J. M. Dell, L. Faraone, T. A. Fisher, G. Parish, Y.-F. Wu, and U. K. Mishra, J. Appl. Phys. **87**(8), 3900 (2000).

[10] S. K. Davidsson, T. G. Andersson, and H. Zirath, Appl. Phys. Lett. **81**, 664 (2002).

[11] S. K. Davidsson, M. Gurusinghe, T. G. Andersson, and H. Zirath, J. Electron. Mater. **33**, 440 (2004).

[12] C. Youtsey, L. T. Romano, R. J. Molnar, and I. Adesida, Appl. Phys. Lett. **74**(23), 3537 (1999).

[13] T. Ando, A. B. Fowler, and F. Stern, Rev. Mod. Phys. **54**(2), 437 (1982).

[14] F. Stern and W. E. Howard, Phys. Rev. **163**(3), 816 (1967).

[15] K. Hirakawa and H. Sakaki, Phys. Rev. B **33**(12), 8291 (1986).

[16] K. Lee, M S. Shur, T. J. Drummond, and H. Morkoc, J. Appl. Phys. **54**(11), 6432 (1983).

[17] L. Hsu and W. Walukiewicz, Phys. Rev. B **56**(3), 1520 (1997).

[18] D. N. Qunang, V. N. Tuoc, and Y. D. Huan, Phys. Rev. B **68**, 195316 (2003).

[19] P. J. Price, Surf. Sci. **113**, 199 (1982).

[20] P. J. Price, Surf. Sci. **143**, 145 (1984).

[21] V. W. L. Chin, T. L. Tansley, and T. Osotchan, J. Appl. Phys. **75**(11), 7365 (1994).

[22] D. C. Look, J. R. Sizelove, S. Keller, Y. F. Wu, C. K. Mishra, and S. P. DenBaars, Solid State Commun. **102**(4), 297 (1997).

[23] O. Ambacher, B. Foutz, J. Smart, J. R. Shealy, N. G. Weimann, K. Chu, M. Murphy, A. J. Sierakowski, W. J. Schaff, L. F. Eastman, R. Dimitrov, A. Mitchell, and M. Stutzmann, J. Appl. Phys. **87**(1), 334 (2000).

[24] I. P. Smorchkova, C. R. Elsas, J. P. Ibbetson, R Vetury, B. Heying, P. Fini, E. Haus, S. P. DenBaars, J. S. Speck, and U. K. Mishra, J. Appl. Phys. **86**(8), 4520 (1999).

[25] E. Frayssinet, W. Knap, P. Lorenzini, N. Grandjean, J. Massies, C. Skierbiszewski, T. Suski, I. Grzegory, S. Porowski, G. Simin, X. Hu, M. A Khan, M. S. Shur, R. Gaska, and D Maude, Appl. Phys. Lett. **77**(16), 2551 (2000).

[26] C. R. Elsass, I. P. Smorchkova, B Heying, E. Haus, P. Fini, K.

Maranowski, J. P. Ibbetson, S. Keller, P. M. Petroff, S. P. DenBaars, U. Mishra, and J. Speck, Appl. Phys. Lett. **74**(23), 3528 (1999).

[27] J. B. Webb, H. Tang, S. Roife, and J. A. Bardwell, Appl. Phys. Lett. **75**(7), 953 (1999).

[28] M. N. Gurusinghe, "Electrical Characterization of GaN and AlGaN/GaN Heterostructures by Molecular Beam Epitaxy," Licentiate thesis, ISSN-0280-2872, Department of Microelectronics and Nanoscience, Chalmers University of Technology and Göteborg University, Sweden, 2002 (unpublished).